PROPAGATION CHARACTERISTICS OF WIDEBAND MIMO CHANNEL IN HOTSPOT AREAS AT 5.25 GHZ

Jianhua Zhang, Xinying Gao, Ping Zhang
Wireless Technology Innovation Institute
Beijing University of Posts and Telecommunication
Beijing, China

Xuefeng Yin
Navigation and Communications (Navcom)
Department of Electronics Systems, Aalborg University
Aalborg, Denmark

ABSTRACT

Wideband channel measurements have been performed at 5.25 GHz in hotspot areas in Beijing with a multiple-input multiple-output channel sounder. The measured scenarios include indoor line-of-sight (LOS) and non-line-of-sight, and outdoor LOS and obstructed-line-of-sight. Statistical results of channel characteristics are presented which include the path loss models, root mean square delay spread, circular azimuth spread and average envelope correlation with respect to antenna separation. Comparative analysis of the results are provided. These information are of significance for the design and performance evaluation of International Mobile Telecommunications (IMT)-Advanced systems.

I INTRODUCTION

Beyond 3G or 4G system has been named officially as "International Mobile Telecommunications (IMT)-Advanced" by ITU-R on Oct. 2005 [1]. For IMT-Advanced systems, the RF bandwidth and carrier frequency are up to 100 MHz and 5 GHz respectively, which are suitable for the hotspot applications that provide super high datarate (up to 1 Gbps) transmission with the limited coverage. Channel measurement is required in order to understand the mechanism of the radio propagation and the characteristics of the radio channel in this scenario. This knowledge is necessary for the design and performance optimization of the IMT-Advanced systems. Recently, we conducted wideband multiple-input multiple-output (MIMO) channel measurements in both indoor and outdoor scenarios in hotspot areas in Beijing, China.

The large-scale fading effects are important for coverage prediction and interference analysis in radio systems. Based on the measured channel impulse responses (CIRs), both the path loss (PL) and shadow fading are modeled with respect to the log-distance. For the delay characteristics of the channel, root mean square (rms) delay spread (DS) is investigated which provides a measure of the variability of excess delay, the coherent bandwidth and frequency selectivity. This study is of great importance for the design of orthogonal frequency division multiplexing (OFDM) techniques, e.g. the length of cyclic prefix (CP), subcarrier spacing. In this contribution, the empirical cumulative density functions (cdfs) of the rms DS are presented for each scenario.

In order to extract the spatial characteristics from the measured data, a Space-Alternating Generalized Expectation-maximization (SAGE) algorithm [2, 3, 4, 5] is utilized to estimate the parameters of multipath components (MPCs) in our investigations. Compared with other algorithms, e.g. the Estimating Signal Parameter via Rotational Invariance Technique (ESPRIT) [6] and the MUltiple SIgnal Classification (MUSIC) [7] method, the SAGE algorithm has no constraints on the array responses, and exhibits the strong ability to detect the weak waves. Based on the angular parameters estimated by SAGE, circular azimuth spread (CAS) is studied for indoor and outdoor scenarios. The envelope correlation, as a function of mean angle of incidence, angle spread and antenna separation distance, are computed from the estimated power azimuth spectrum (PAS).

The rest of the paper is organized as follows. The measurement system and the environment are described briefly in Section II Channel characteristics are presented in four perspectives, i.e. PL, rms DS, CAS and envelope correlation in Section III Finally, conclusions are drawn in Section IV

II CHANNEL MEASUREMENT CAMPAIGN

A *Measurement System*

Extensive channel measurements were performed at the center carrier frequency of 5.25 GHz with 100 MHz bandwidth at Beijing University of Posts and Telecommunications (BUPT), China. The measured data were collected using the MIMO channel sounder PropSound [8], which uses the pseudo random binary signals (PRBS) and the time-division multiplexed (TDM) switching of the multiple transmit and receive antennas. The transmitted power was 26 dBm and the lengths of the PRBS were 511 and 1022 for indoor and outdoor measurements, respectively. The transmitter (Tx) was equipped with a dual-polarized omni-directional array (ODA) with maximum 50 elements. The receiver (Rx) employed a vertically polarized 8-element uniform circular array (UCA). Fig. 1 (a) and (b) depict respectively the configurations of the Tx and Rx antenna arrays. The spacing between the neighboring antennas in the ODA and the UCA is half-a-wavelength.

B *Measurement Environment*

Static measurements were conducted in a 7-floor building for the indoor scenario. The dimension of each floor is 120 m $\times$ 45 m $\times$ 6 m. The Tx array and the Rx array were located about 1.5 m and 2.5 m above the floor level respectively. All the elements in the Tx and the Rx arrays are used in the indoor measurements. Fig. 2 (a) illustrates the map of the first floor where the measurement campaign was conducted. During all the measurements, the Rx was fixed at the position marked with

The research is funded by National 863 High Technology Research and Development Program of China (No. 2006AA01Z258) and Motorola Ltd.

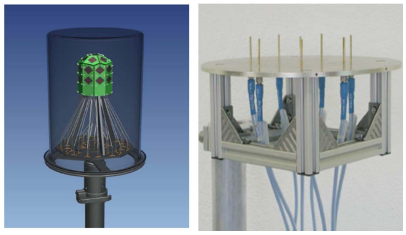

(a) (b)

Figure 1: Configurations of the antenna arrays used in the measurements: (a) Tx array; (b) Rx array

the arrow denoting the reference direction. For the LOS measurements, the Tx was moved following the grids marked with dots in the area "Grid A". For the NLOS scenarios, the Tx was moved following the dots marked in the area "Grid B". The height of the ceiling in the areas "Grid A", "Grid B", as well as at the position of the Rx is only 3 m. The walls along the corridor and between the rooms are made of bricks with plasterboard on the surface. The floor is covered with marbles. The doors of the rooms are wooden. The entrance doors are made of glass with aluminum frames. Between the Rx and the "Gird B" area, there are concrete pillars, escalators, staircases with aluminum banisters, notice boards with glass sheets, etc.

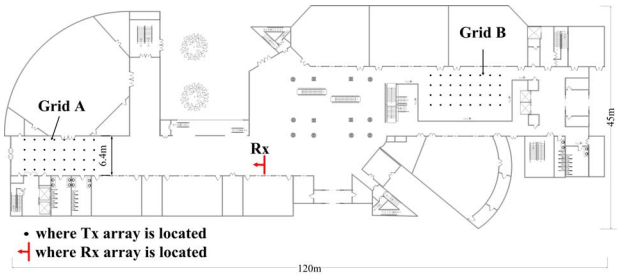

(a)

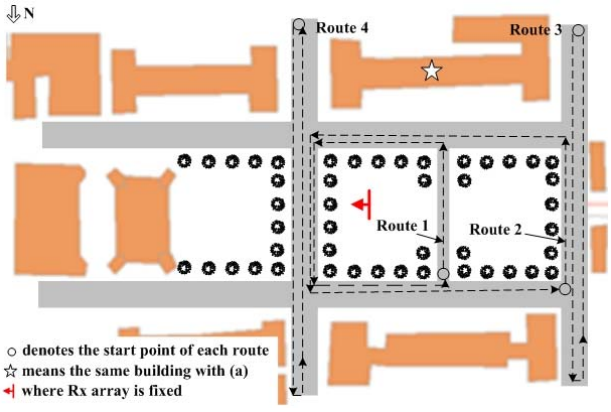

(b)

Figure 2: Measurement environments and scenarios: (a) Top views of indoor scenario; (b) Measurement routes in the outdoor scenario

For the outdoor hotspot scenario, mobile measurements were conducted following four routes along the streets. These routes are marked as the dashed lines in Fig. 2 (b). The lengths of these routes were from 380 m to 520 m. The Rx was fixed with antenna height of about 2.5 m and marked with the arrow denoting the reference direction. The Tx was mounted on the top of a car with the vehicle speed of nearly 20 km/h. Totally 18 elements of the Tx array are used which have identical height of about 2.75 m. The streets are bordered by trees, and the Rx was surrounded by trees, grasses, two sculptures made of stone, lamp poles, etc. The propagation in this scenario can be categorized as LOS/OLOS. During the measurements, the Tx positions along the routes were recorded using the Global Positioning System (GPS).

III Propagation Characteristics

In order to satisfy the wide-sense stationary and uncorrelated scattering (WSSUS) condition, the CIRs for a sub-channel are divided into subsets, and averaged according to

$$h_{\mathrm{av}}(\tau) = \mathrm{E}_t\{h(t,\tau)\}, \tag{1}$$

where $\mathrm{E}_t\{\cdot\}$ denotes the average in time domain. In the mobile measurements, the time span for averaging corresponds to a suitable window length around 20λ [9] (about 1.15 m) with λ denoting the carrier wavelength. In the static measurements, the averaging is performed using 100 snapshots at each measurement location. The dynamic range used in the SAGE algorithm is set as 30 dB for indoor LOS, 25 dB for indoor NLOS, and 15 dB for outdoor measurements, respectively.

A Path Loss Models

After averaging and delay search, the measured PL values are calculated in dB according to:

$$PL = -10\log_{10}\left(\int_{\tau}|h_{\mathrm{av}}(\tau)|^2 d\tau\right) + G_{\mathrm{Tx}} + G_{\mathrm{Rx}}, \tag{2}$$

where G_{Tx} and G_{Rx} denote respectively, the gains of the underlying Tx and Rx antenna. The values of G_{Tx} and G_{Rx} can be calculated from the antenna calibration response. To extract the large-scale characteristics, a linear curve fitting method is used which fits the decibel path loss to the decibel distance with a random variation. The empirical model of log-distance PL described in [10] is written as

$$PL(d) = PL_0 + 10n \cdot \log_{10}(d) + X_\sigma, \tag{3}$$

where PL_0 represents the intercept, d embodies the spacing of the Tx and the Rx expressed in meters, and n denotes the PL exponent which indicates the rate that PL increases with respect to the distance. The value of n is dependent on the specific propagation environment. Considering the fact that with the same Tx-Rx spacing, the surroundings of the Tx and the Rx in one scenario might be vastly different from those in another scenario, the log-normal shadow fading is denoted using a zero-mean Gaussian random variable X_σ with standard deviation σ.

The values of PL_0 and n are identified by using the least squares (LS) method. For comparison purpose, the PL model

in the scenario of free space propagation, i.e.

$$PL_{\mathrm{FS}}(d) = 20\log_{10}\left(\frac{4\pi d}{\lambda}\right) \quad (4)$$

given by Friis equation [11], is considered. The antenna gains are excluded. This model is used to predict the received signal strength when the transmitter and receiver have a clear, unobstructed LOS path between them. In this case the PL exponent n equals 2.

1) Indoor LOS and NLOS Scenario

Fig. 3 reports these two PL models on the first floor. For the LOS scenario, the exponent is calculated to be 1.18, which is smaller than 2 in the free space propagation scenario. This is reasonable since in the rich scattered environment, there're a number of MPCs besides the LOS path as specified in the free space. Another reason might be the waveguide effect of the corridor where the Tx and Rx were located. For the NLOS case, the exponent equals 4.33 with standard deviation of 1.1 dB. Transited from LOS to NLOS around 40 m Tx-Rx distance, the difference between the propagation PLs is about 26.5 dB. Since the exponent of NLOS is much larger than that of LOS, this increment will increase with Tx-Rx distance beyond 40 m.

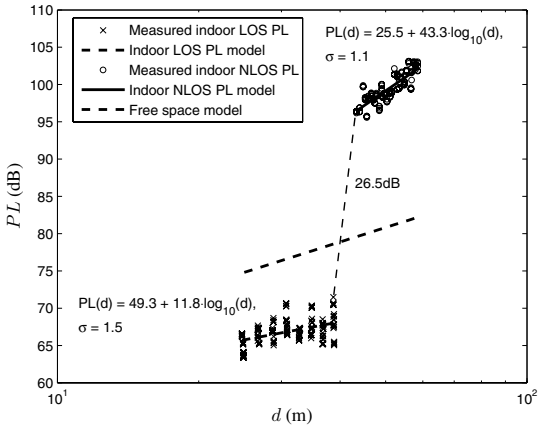

Figure 3: Empirical PL models in the indoor scenario

2) Outdoor LOS/OLOS Scenario

Using the measurement data collected in the outdoor scenarios (see Fig. 2 (b)), an empirical PL model is computed for the LOS/OLOS propagation, i.e.

$$PL(d) = 47.2 + 23.2 \cdot \log_{10} d, \quad (5)$$

The standard deviation of shadow fading is measured to be 6.0 dB. The valid Tx-Rx spacing ranges from 30 m to 200 m. Fig. 4 depicts the measured PL and the graph of the PL model. Compared with the free space, the exponent of outdoor is 2.32, and the PL values are larger than that of free space over the measured Tx-Rx distance. This result indicates that some obstructed scatterers might absorb a certain mount of power, and further demonstrates the waveguide effect available in indoor corridor.

Since both the Tx and Rx arrays have low heights, the obtained PL model is different from the results observed using the traditional microcellular system where the base station is usually equipped with antennas much higher than those in the mobile stations, e.g. by 5 m to 15 m. This model can be used in the design of peer-to-peer communication systems [12] and cooperative transmission [13] for the next generation wireless network.

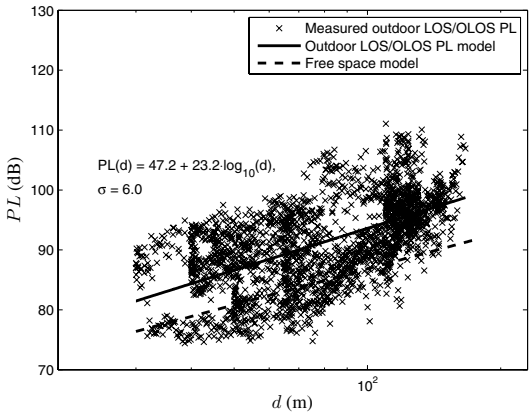

Figure 4: Empirical PL model in the outdoor scenario

B Delay Spread

The rms DS τ_{rms} is calculated to be the standard deviation of the excess delay weighted with the power, i.e.

$$\tau_{\mathrm{rms}} = \sqrt{\left(\sum_{\ell=1}^{L} P_\ell\right)^{-1} \sum_{\ell=1}^{L} \tau_\ell^2 P_\ell - \left(\sum_{\ell=1}^{L} P_\ell\right)^{-2} \left(\sum_{\ell=1}^{L} \tau_\ell P_\ell\right)^2}, \quad (6)$$

where τ_ℓ and P_ℓ denote respectively, the excess delay and the power of the ℓth path. The mean DS in indoor LOS, indoor NLOS, and outdoor LOS/OLOS scenarios is calculated to be 26.7 ns, 39.6 ns and 43.8 ns, respectively. Fig. 5 shows the graphs of the rms DS cdfs and the fitted log-normal distributions $\tau_{\mathrm{rms}} = 10^{\mu_D + X\sigma_D}$. Here, X denotes a zero-mean Gaussian random variable with unit variance, $\mu_D = \mathrm{E}\{\log_{10}(\tau_{\mathrm{rms}})\}$ and $\sigma_D = \mathrm{std}\{\log_{10}(\tau_{\mathrm{rms}})\}$ represent respectively, the mean and the standard deviation of logarithmic rms DSs. At the probability lower than 60 %, the rms DS is smaller in the outdoor scenarios than in the indoor NLOS case, due to the reason that the coverage of scattering environment involved in route 1 and route 2 is much limited, resulting in the lower spread of MPCs.

C Angle Spread

To evaluate the angle of departure (AoD) and angle of arrival (AoA) numerically, the azimuth spread is calculated as the root second central moment of the PAS. To avoid the ambiguous effect due to the circular wrapping of the angles, the circular AS is calculated. This AS is constant regardless of the value

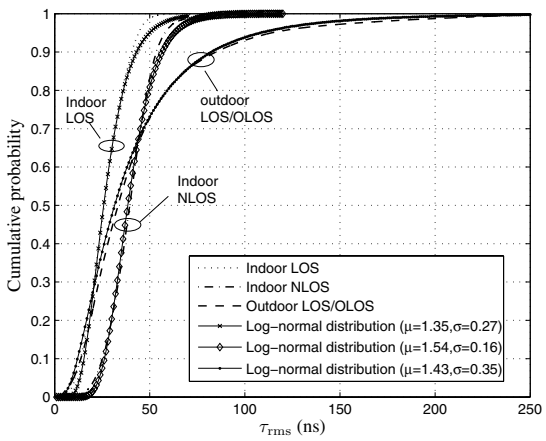

Figure 5: Empirical cdfs and fitted log-normal distribution of rms DS

of the angle origin, as in the case described in the 3GPP spatial channel model (SCM) specification [14].

Table 1 depicts the statistics of the CAS obtained from the measurements. In the table, μ_A and σ_A are the parameters of the log-normal distributions when they are fitted to the CAS observations. The results obtained in the indoor scenarios demonstrate that the CAS in the NLOS case is only slightly larger than the CAS in the LOS scenario. One reason resulting in this effect could be due to the fact that the omni-direction antenna array was used in the Tx. As a consequence, in the LOS case, the multipath effect is still significant due to the reflections and scattering of the ceiling, floor, walls and other objects in the environment. Compared with AoD, the CAS of AoA is a bit larger, especially for the NLOS cases. Further measurements in small offices also demonstrate the similar observation. It appears that for the considered indoor environments, the CAS decreases when the antenna height increases. It can also be observed that the value of σ_A obtained in the outdoor scenarios is much larger than that observed in the indoor scenario. Similarly, in the outdoor scenarios, the mean CAS of AoA is much larger than the mean CAS of AoD. This is reasonable as in the considered outdoor environment, the Rx was fixed in an environment with much richer scattering than that of the Tx along the mobile routes.

Table 1: Statistics of CAS obtained from measurements.

Scenarios		Indoor		Outdoor
		LOS	NLOS	LOS/NLOS
CAS of AoD	$\mu_A(\log_{10}(^\circ))$	1.58	1.61	1.24
	$\sigma_A(\log_{10}(^\circ))$	0.22	0.16	0.65
	Mean $(^\circ)$	38.0	40.7	17.4
CAS of AoA	$\mu_A(\log_{10}(^\circ))$	1.59	1.71	1.58
	$\sigma_A(\log_{10}(^\circ))$	0.18	0.25	0.46
	Mean $(^\circ)$	38.9	51.3	38.0

D Envelope Correlation

It has been shown [15] that the envelope correlation of the outputs of two antennas can be approximated by the magnitude squared of the complex correlation that can be calculated from the PAS. According to [16], the complex correlation can be computed to be

$$R(d) = \int_{\bar{\phi}-\sigma}^{\bar{\phi}+\sigma} \exp\{j2\pi d \sin(\phi)\} p(\phi) \mathrm{d}\phi, \qquad (7)$$

where d is the antenna separation distance in wavelengths, and $p(\phi)$ denotes the normalized PAS in ϕ. The expression (7) is independent of the structure of the underlying antenna array. The envelope correlation $\rho(d)$ can be approximated as $\rho(d) \approx |R(d)|^2$. In order to obtain an acceptable diversity gain [17], it is generally required $\rho \leq 0.7$. The antenna separation d for $\rho = 0.7$ is known as the correlation distance. In this contribution, we consider the azimuth only. In this case, the parameter d is referred to as the horizontal antenna spacing. It should be noted that the spatial correlation has the non-isotropic property [18] due to $\bar{\phi}$, particularly for the mobile terminal with random orientations.

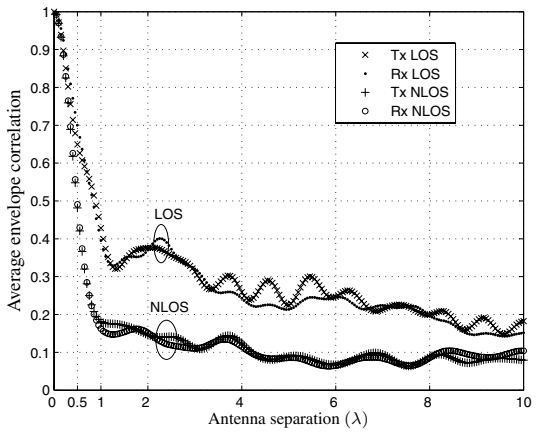

Figure 6: Average envelope correlation in the indoor scenario

Fig. 6 depicts the average envelope correlation with respect to the antenna separation for indoor measurements. The average correlation is similar for the Tx and Rx sites in both the LOS and the NLOS scenarios. The average correlation distances are observed to be 0.38λ for both the Tx and Rx in the NLOS scenario, 0.4λ for the Tx and 0.5λ for the Rx in the LOS scenario. Fig. 7 demonstrates the average envelope correlation in the outdoor measurement. It can be observed that the average correlation for Tx is similar with that for Rx. The correlation distance is obtained as 0.5λ. From the results above, it's observable that both in indoor and outdoor with low antenna heights, 0.5λ antenna separation is sufficient to obtain correlation less than 0.7. This result is important for calculating the capacity limits and MIMO system design in the hotspot areas.

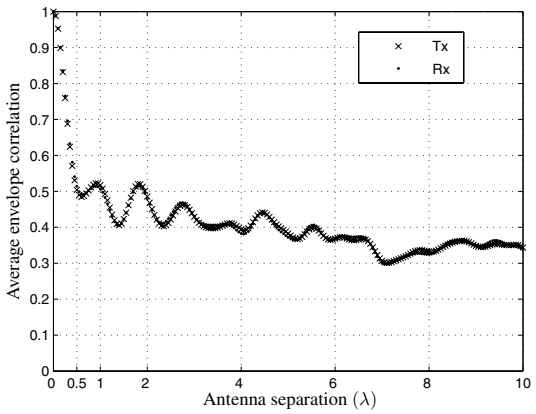

Figure 7: Average envelope correlation in the outdoor scenario

IV Conclusions

In this contribution, the characteristics of the radio channel at 5.25 GHz are investigated using measurement data collected in the hotspot areas in Beijing, China. Based on the measurements, the empirical log-distance PL models are established with the path loss exponents of 1.18, 4.33, and 2.32 for indoor LOS, NLOS, and outdoor LOS/OLOS, respectively. The cdf statistics of the rms DS and CAS demonstrate no large difference between indoor and outdoor measurements with similar Tx and Rx antenna height. The results of average envelope correlation indicate that for the considered environments, the antenna separation of half-a-wavelength is large enough to achieve 0.7 envelope correlation both in indoor and outdoor scenarios. These results can be used to design the MIMO systems, particularly the IMT-Advanced systems for hotspot applications.

V Acknowledgements

The authors would like to thank the engineers of Elektrobit, Finland for their efforts in the measurement campaign. Useful help and discussions from Jukka-Pekka Nuutinen and Troels Pedersen are greatly appreciated.

References

[1] "Naming for systems beyond IMT-2000," ITU-R WP8F, Tech. Rep., Oct. 2005.

[2] B. H. Fleury, M. Tschudin, R. Heddergott, D. Dahlhaus, and K. L. Pedersen, "Channel parameter estimation in mobile radio environments using the SAGE algorithm," *IEEE J. Select. Areas Commun.*, vol. 17, no. 3, pp. 434–450, Mar. 1999.

[3] B. H. Fleury, X. Yin, K. G. Rohbrandt, P. Jourdan, and A. Stucki, "Performance of a high-resolution scheme for joint estimation of delay and bidirection dispersion in the radio channel," in *Proceedings of the IEEE Vehicular Technology Conference (VTC-Spring)*, vol. 1, May 2002, pp. 522–526.

[4] B. H. Fleury, P. Jourdan, and A. Stucki, "High-resolution channel parameter estimation for MIMO applications using the SAGE algorithm," in *Proceedings of International Zurich Seminar on Broadband Communications*, vol. 30, Zurich, Switzerland, Feb. 2002, pp. 1–9.

[5] B. H. Fleury, X. Yin, P. Jourdan, and A. Stucki, "High-resolution channel parameter estimation for communication systems equipped with antenna arrays," in *Proceedings of the 13th IFAC Symposium on System Identification (SYSID)*, no. ISC-379, Rotterdam, The Netherlands, 2003.

[6] R. Roy and T. Kailath, "ESPRIT - Estimation of Signal Parameters via Rotational Invariance Techniques," *IEEE Trans. Acoust., Speech, Signal Processing*, vol. 37, no. 7, pp. 984–995, July 1989.

[7] R. O. Schmidt, "Multiple emitter location and signal parameter estimation," *IEEE Trans. Antennas. Propagat.*, vol. 34, no. 3, pp. 276–280, Mar. 1986.

[8] A. Stucki *et. al.*, "PropSound System Specifications Document: Concept and Specifications," Elektrobit AG, Switzerland, Tech. Rep., 2001.

[9] X. Zhao, J. Kivinen, P. Vainikainen, and K. Skog, "Propagation characteristics for wideband outdoor mobile communications at 5.3 GHz," *IEEE J. Sel. Areas Commun.*, vol. 20, pp. 507–514, 2002.

[10] V. Erceg, L. J. Greenstein, S. Y. Tjandra, S. R. Parkoff, A. Gupta, B. Kulic, A. A. Julius, and R. Bianchi, "An empirically based path loss model for wireless channels in suburban environments," *IEEE J. Sel. Areas Commun.*, vol. 17, pp. 1205–1211, 1999.

[11] T. S. Rappaport, *Wireless Communications: Principles & Practice*. Upper Saddle River, NJ, Prentice Hall PTR, 1996.

[12] H. Wu, C. Qiao, S. De, and O. Tonguz, "Integrated cellular and Ad hoc Relaying systems: iCAR," *IEEE J. Sel. Areas Commun.*, vol. 19, no. 10, pp. 2105–2115, 2001.

[13] R. Pabst, B. Walke, D. Schultz, and P. Herhold, "Relay-based deployment concepts for wireless and mobile broadband cellular radio," *IEEE Commun. Mag*, vol. 42, pp. 80–89, 2004.

[14] 3GPP, "TR 25.996 spatial channel model for Multiple Input Multiple Output (MIMO) simulations, v6.1.0," Tech. Rep., 2003-09.

[15] R. G. Vaughan and J. B. Andersen, "Antenna diversity in mobile communications," *IEEE Trans. Veh. Technol.*, vol. 36, pp. 149–172, 1987.

[16] W. Lee, "Effects on correlation between two mobile radio base-station antennas," *IEEE Trans. on Communications*, vol. 21, no. 11, pp. 1214–1224, 1973.

[17] R. O. LaMaire and M. Zorzi, "Effect on correlation in diversity systems with Rayleigh fading, shadowing, and power capture," *IEEE J. Select. Areas Commun.*, vol. 14, pp. 449–460, 1996.

[18] D. D. Gregory and T. S. Rappaport, "Effects of multipath angular spread on the spatial cross-correlation of received voltage envelopes," in *Proceedings of the IEEE Vehicular Technology Conference (VTC-Spring)*, vol. 2, May 1999, pp. 996–1000.